JOURNAL OF MATERIALS SCIENCE 37 (2002) 637–647

The formation, structural, electrical, magnetic and Mössbauer properties of ferrispinels, $Cd_{1-x}Ni_xFe_2O_4$

A. K. NIKUMBH*, A. V. NAGAWADE, G. S. GUGALE, M. G. CHASKAR, P. P. BAKARE
Department of Chemistry, University of Pune, Ganeshkhind, Pune 411 007, India
E-mail: aknik@chem.unipune.ernet.in

A series of $Cd_{1-x}Ni_xFe_2O_4$ (where $x = 0.0$, 0.2, 0.4, 0.6, 0.8 and 1.0) were synthesized by the tartarate precursor method. The formation of these ferrispinels was studied by X-ray powder diffraction, infrared spectroscopy, electrical conductivity, thermoelectric power, magnetic hysteresis, initial magnetic susceptibility and Mössbauer spectroscopy. The temperature variation of the direct current electrical conductivity showed a definite kink (break) in the range 645 to 806 K except for $x = 0$ and $x = 0.2$ samples. The kink occurred in each curve ($x \geq 0.4$) at a temperature which corresponds to the ferrimagnetic to paramagnetic transition. The thermoelectric power for all samples was negative over the whole range of temperature, indicating that the charge carriers are electrons (i.e. n-type semiconductivity). The compounds with $x \geq 0.4$ showed a definite hysteresis loop. The composition dependence of the saturation magnetization (M_S) and magnetic moment (n_B) up to $x = 0.8$, has been explained on the basis of the existence of Yafet–Kittel angles on the B-site spins. The Néel's two sublattice model can be applied to the sample with $x = 1$. The Mössbauer spectra of compounds with $x = 0.0$ and 0.2 showed a paramagnetic doublet, while $x = 0.4$ and 0.6 exhibited a relaxation spectrum. The compounds with $x \geq 0.8$ exhibited normal Zeeman split sextets at room temperature.

1. Introduction

Ferrites are a group of technologically important materials. Substituted nickel ferrites have been the subject of extensive investigation because of their microwave applications. The method of preparation plays a very important role with regard to the chemical, structural and magnetic properties of a mixed spinel ferrites [1–8].

A number of methods are known in the preparation of mixed oxide spinels. The most common among them is the ceramic technique [9], in which the oxides, hydroxides, carbonates, nitrates or oxalates of metals are used as the starting compounds. In wet methods-coprecipitation and oxidation reactions [10, 11] and the low temperature decomposition of adequate precursor compounds-including phases as oxalates [12, 13], carbonates [14], hydroxynitrates [15], hydrazine carboxylate hydrates [16] and organometallic polymers [17].

The study of intrinsic properties of materials has led to important new ideas concerning the origin and nature of magnetic phenomena. It seems reasonable that fundamental physical studies should be made on compounds of the highest available purity and homogeneity. Formation of $Cd_{1-x}Ni_xFe_2O_4$ solid solution needs a temperature range, which, unfortunately, is concurrent to that one of the cadmium oxide volatility. This leads to product with various degrees of deviation from stoichiometry and hence, probably, to inconsistency in information on the magnetic properties for that series [18].

In the present work the investigations were made using coprecipitated tartarates of general composition $Cd_{1-x}Ni_xFe_2(C_4H_4O_6)_3 \cdot nH_2O$ $(0 \leq x \leq 1)$. We attempted to determine the effect of cadmium ferrite spinel formation and the role of nickel content on structural and electrical properties of these ferrispinels. The magnetic measurements were also undertaken to study the variation of satuaration magnetization and hyperfine fields with nickel concentration and to gain information about the cation distribution, possible canted spin structures and supertransferred hyperfine interactions at both A and B sites in the system.

2. Experimental

2.1. Synthesis of precursors

Cadmium–iron–tartarate $(CdFe_2(C_4H_4O_6)_3 \cdot 5H_2O)$ was prepared according to the similar procedure described in ref. 19.

* Author to whom to all correspondence should be addressed.

Nickel–iron–tartarates were prepared by the co-precipitation method. A high purity (reagent grade) mixture of $NiSO_4 \cdot 6H_2O$ (1.11×10^{-1}M/L) and $FeSO_4 \cdot 7H_2O$ (2.22×10^{-1}M/L) were dissolved in deionized water. The mixture of metal-sulphate solution was prepared in ratio of $Ni^{2+} : Fe^{2+} = 1 : 2$ with respect to molar ratios and was placed in a three-naked flask under a stream of dry nitrogen. The pH of the medium was adjusted to a low enough value (pH < 6), so that hydroxide precipitate does not form. The solution was stirred vigorously with a magnetic stirrer. The temperature of the solution was maintained at about 50°C. The sodium tartarate (7.0%) solution was then added slowly with stirring till a permanent precipitate occured. Acetone was added in equal amounts to metal salts. Here addition of acetone not only ensures a high yield but also influences more homogeneous, stoichiometric, fine-grained powders. The resultant precipitate of $NiFe_2(C_4H_4O_6)_3 \cdot 5H_2O$ was greenish yellow in colour. The solution was filtered after stirring it for 30 minutes. The precipitate was washed several times with cold distilled water and then with acetone to speed-up drying. The precipitate was dried at ambient temperature.

The similar experimental conditions was used for the preparation of mixed nickel–cadmium–iron tartarates, $Ni_xCd_{1-x}Fe_2(C_4H_4O_6)_3 \cdot nH_2O$.

2.2. Synthesis of nickel-cadmium ferrites $Cd_{1-x}Ni_xFe_2O_4$

For the synthesis of $Cd_{1-x}Ni_xFe_2O_4$ ($x = 0.0$ to 1.0), the above tartarate coprecipitates were decomposed and calcined slowly at 700°C for two hours in a platinum crucible under static air atmosphere and then slowly cooled (3°C/min) down to room temperature. This heat treatment is sufficient for achieving a complete decomposition of tartarate. The powder obtained was polycrystallite. This sample was then reground and recalcined at the same temperature for another two hours. The furnace was turned off and sample was removed at room temperature. These samples were stored in a desiccator.

2.3. Chemical analysis

The chemical analysis was done using a Perkin-Elmer Model 3100 Atomic Absorption Spectrometer (AAS) employing an air acetylene flame and a hollow cathode lamp as the light source. The duplicate samples (known amount of $Cd_{1-x}Ni_xFe_2O_4$ samples dissolved in 2 ml concentrated HCl and 5 ml HNO_3. The final volume was made to 100 ml) were used for this analysis. A separate lamp was used for the determination of each element. A blank solution (distilled water) was run before and after the aspiration of every sample into flame.

2.4. X-ray diffraction studies

The nickel–cadmium ferrites ($Cd_{1-x}Ni_xFe_2O_4$) were analysed by X-ray powder diffraction techniques using Cu K_α radiation ($\lambda = 1.5405$ A°; nickel filter) on a PW 1730 Philips X-ray diffractometer. To measure the intensity, the area under different (hkl) peaks were determined and the values obtained in relation to the peak area for the 311 reflection which is taken to represent 100. To ensure the reliability of the method, the compounds (i.e. $Cd_{1-x}Ni_xFe_2O_4$) were subjected to X-ray diffractometry twice and, after correction for background, a mean value of area was taken (reproducible to within 2%). To calculate the relative integrated intensity, I, of a given (hkl) reflection, the Buerger [20] formula is used. These were then compared with the observed intensity ratios. The maximum standard deviation in the observed ratios is ±0.02.

The experimentally observed d-spacing values and relative intensities were then compared with those reported in the ASTM File. After determining the d values, the unit cell of the lattice constant 'a' for cubic system was calculated using the following equation:

$$d = \frac{a}{\sqrt{h^2 + k^2 + l^2}}$$

Here k, k and l are miller indices for the reflecting lattice planes.

2.5. Infrared spectroscopy study

Infrared spectra were recorded on a Perkin Elmer Model 2000 spectrophotometer using KBr discs.

2.6. Direct current electrical conductivity measurements

The direct current (d.c.) electrical conductivity, σ, measurement was measured by the two-probe method. The sample (i.e. $Cd_{1-x}Ni_xFe_2O_4$), in the form of a pellet weight: 1.00 g; diameter: 10 mm; thickness: 3.5 ± 0.2 mm; pressure at which the pellet was formed: 2.0×10^2 Kg cm^{-2} was pressed between two spring-loaded platinum electrodes and the resistivity was measured in the usual manner by measuring the difference in potential between the electrodes for a known current across the specimen. The potential developed between the potential probes was measured using a Philips PP 9004 microvoltmeter. For direct measurement of resistance the Philips GM 6009 Ohmmeter was used. The specific conductivity was obtained by taking into consideration the dimensions of probe and sample.

The conductivity cell was designed so that different atmospheres could be used. The cell was kept in a tubular furnace whose temperature was controlled within ±1°C. A precalibrated Chromel–Alumel thermocouple was used for sensing the temperature (±0.1°C). Philips PP 9004 microvoltmeter was used to read the potential developed between the hot zone and the cold zone (ice water).

The conductivity data are presented as log σ against $10^3\ T^{-1}\ (K^{-1})$. The data were determined using three different pellets of the same sample, and it was observed that the pattern of the σ - T^{-1} plots were reproducible to within ±1°C.

2.7. Thermoelectric power measurements

The $Cd_{1-x}Ni_xFe_2O_4$ sample in the form of a pellet of 10 mm thickness was pressed between two platinum disks fixed at the ends of two ceramic blocks. One of these blocks was spring - loaded to obtain good pressure contact. This sample holder along with the sample was placed in a constant temperature zone of a furnace, whose temperature was held to within $\pm 1^{\circ}$C. The temperature of the ends of the sample were measured with Chromel–Alumel thermocouples, placed in such a way as to touch the sample ends. These junctions were insulated from the platinum disks and ceramic block by means of thin mica sheets. During the measurements, the sample was equilibrated at each temperature for about 10 to 15 min. Temperature differences of 2 to 20°C were used along the sample. The thermoelectric voltage (or Seebeck voltage) developed across the sample and the temperature of the sample ends were read on a Philips PP 9004 microvoltmeter. A set of the values of thermoelectric voltage at various temperatures thus obtained ($\mu V K^{-1}$) was plotted against the respective absolute temperatures. The predominant charge carriers in a temperature gradient diffuse towards the cold end of the sample. The sign of the probe at the lower temperature is the sign of the Seebeck voltage.

2.8. Magnetic hysteresis measurements

The hysteresis studies were made using an alternating electromagnet-type hysteresis loop tracer similar to that described by Likhite *et al*. [21]. The instrument was calibrated for the magnetization measurements using pure nickel (99.9% pure) as the standard.

2.9. Initial magnetic susceptibility study

The measurements of temperature variation of initial magnetic susceptibility were determined by a double-coil method [22, 23], using a field of 1.0 Oe, and a frequency of 263 Hz. The temperature was varied between 20 and 600°C, and was measured accurately within $\pm 1^{\circ}$C.

2.10. Mössbauer spectroscopy study

The constant acceleration Mössbauer spectrometer (Austin Science S-600) assembled in the National Chemical Laboratory (NCL), Pune, was used to record the Mössbauer data in conjunction with 10 mCi ^{57}Co in a rhodium source. The spectrometer was calibrated using a natural iron foil. All the spectra were recorded at 298 ± 2K. A sample containing approximately 10 mg cm^{-2} of natural iron was taken for each measurements. The hyperfine interaction parameter were computed using an interactive least square "MOSFIT" program.

3. Results and discussion

3.1. Characterization of precursors

The elemental analyses of tartarate precursors were made in wt% for $CdFe_2(C_4H_4O_6)_3 \cdot 5H_2O$ (C, 18.58 (18.99); H, 3.01 (2.90); Cd, 15.05 (14.82); Fe, 14.34 (14.73)) and for $NiFe_2(C_4H_4O_6)_3 \cdot 5H_2O$ (C, 20.08 (20.44); H, 3.54 (3.12); Ni, 8.06 (8.33); Fe, 15.41 (15.85)), where the values in parenthesis are calculated ones. The presence of water of crystallization for these precursors was confirmed on the basis of the thermal analysis curves under static air atmosphere. These results are further supplemented by infrared spectroscopic measurements. The bidentate linkage of tartarate group with metal was confirmed on the basis of the difference between the antisymmetric and symmetric stretching frequencies. There was no bonding with secondary - OH group (of d-tartaric acid) to metal in solid state [24, 25]. A chain-like polymeric octahedral structure has been assigned by infrared spectra for these precursors.

Thermal decomposition of the precursors shows that all the complexes dehydrate and decompose in the temperature range 60–400°C. It is observed that the weight loss in TGA corresponds to the formation of Cd-Ni ferrites, $Cd_{1-x}Ni_xFe_2O_4$.

TABLE I Chemical analysis of $Cd_{1-x}Ni_xFe_2O_4$ system ($0 \leq x \leq 1$)

	Wt% of (±0.5)					
	Fe		Cd		Ni	
Compounds	Found	Req.	Found	Req.	Found	Req.
$CdFe_2O_4$	39.02	38.77	38.81	39.01	–	–
$Cd_{0.8}Ni_{0.2}Fe_2O_4$	40.17	40.54	31.02	31.21	4.80	5.00
$Cd_{0.6}Ni_{0.4}Fe_2O_4$	42.00	42.32	23.15	23.40	9.78	10.01
$Cd_{0.4}Ni_{0.6}Fe_2O_4$	43.85	44.09	15.25	15.60	14.82	15.02
$Cd_{0.2}Ni_{0.8}Fe_2O_4$	45.55	45.87	7.68	7.80	19.73	20.03
$NiFe_2O_4$	47.42	47.65	–	–	24.80	25.04

3.2. Characterization of mixed ferrispinels, $Cd_{1-x}Ni_xFe_2O_4$

3.2.1. Compositional analysis

The composition of $Cd_{1-x}Ni_xFe_2O_4$ is characterized at first stage by atomic absorption spectrometry (AAS). The observed compositions are summarized in Table I. They are found to be ±0.5% of the nominated values. The results of chemical analysis showed that ($Cd_{1-x}Ni_x$: Fe) ratio is 1 : 2 within the experimental errors (<1.0%).

3.2.2. X-ray diffraction studies

The X-ray diffraction patterns of $Cd_{1-x}Ni_xFe_2O_4$ ($0 \leq x \leq 1$) are shown in Fig. 1. The X-ray patterns of all the compositions indicate the formation of a single spinel phase with cubic structure. The experimentally observed d-spacing values and relative intensities were compared with those reported in literature [26, 27]. The lattice parameters for each composition were then calculated and are shown in Table II. The lattice constant values are in the expected range with the lattice constants of $CdFe_2O_4$ [26, 28] and $NiFe_2O_4$ [27, 28] at either end.

The variation of lattice parameter 'a' as a function of nickel addition x in $Cd_{1-x}Ni_xFe_2O_4$ is represented in

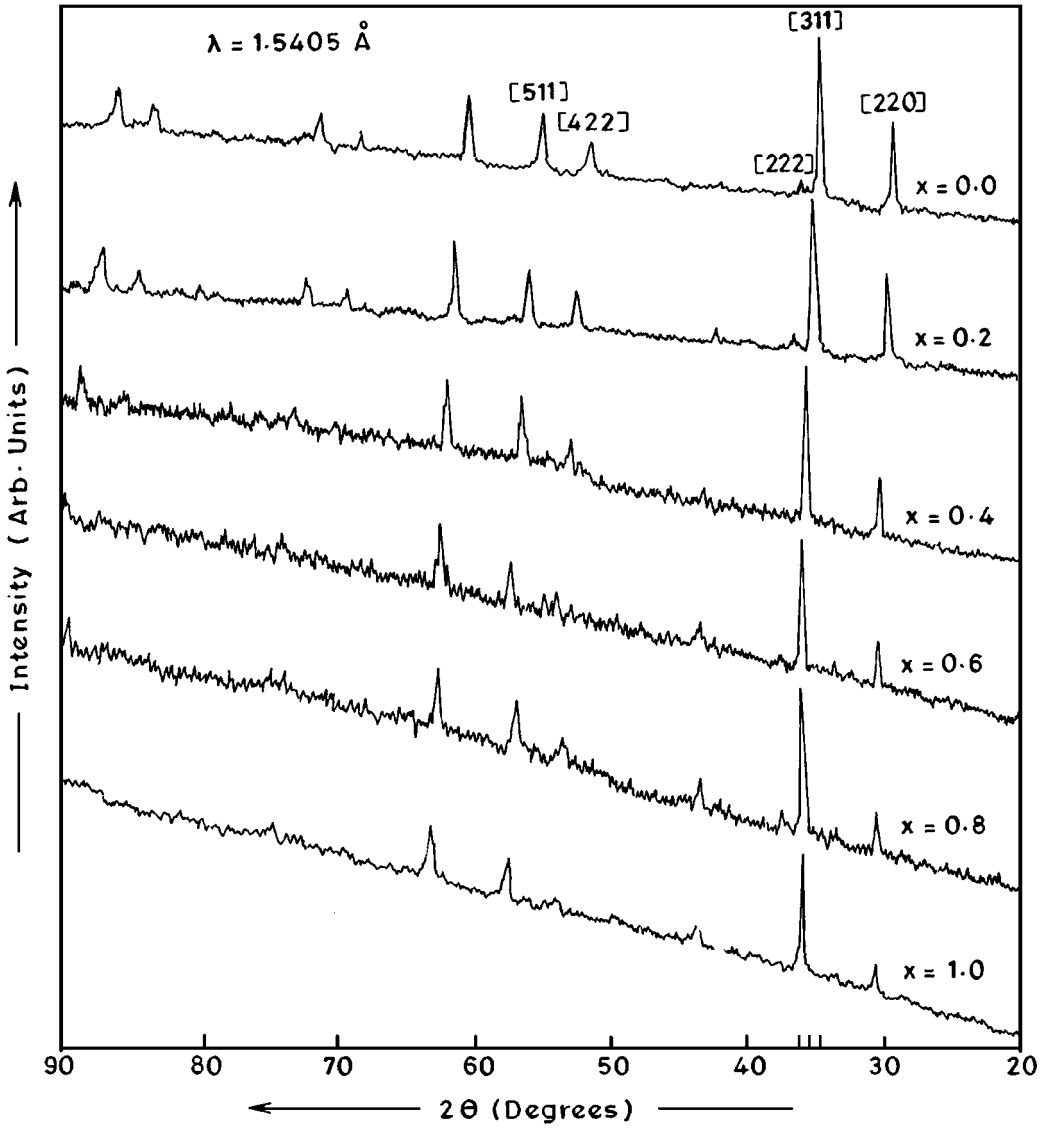

Figure 1 X-ray powder diffraction pattern of $Cd_{1-x}Ni_xFe_2O_4$ system ($0 \leq x \leq 1$).

Fig. 2. It shows that the lattice parameter decreases linearly with the increase of nickel content. The electronic configuration of Cd^{2+} ions have a special preference for tetrahedral coordination. Our results are explained on the assumption that substituting Ni^{2+} ions for Cd^{2+} ions in the composition causes the movement of Fe^{3+} ions from the octahedral sites to tetrahedral sites. The decrease in lattice constant is also due to the replacement of larger Cd^{2+} (ionic radius = 0.092 nm) by comparatively smaller Fe^{3+} in tetrahedral site. Usually in a solid solution of spinels within the miscibility range, a linear change in the lattice constant with concentration of components (Vegard's law) [29] is observed. Non linear behaviour on the other hand, has been reported for the systems which are not completely normal or inverse spinel [30].

3.2.3. Particulate properties

The initial step in the sample evaluation is the measurement of sample density. Using the values of lattice parameter, we calculated X-ray density, D_X (true density) from the relation.

$$D_X = \frac{8M}{Na^3}$$

where M is the molecular weight of the sample, N is Avogadro's number and a is the lattice parameter which is calculated from the X-ray diffraction pattern. The porosity (p) of the sample is also calculated from relation

$$P = 1 - \frac{D}{D_X}$$

where D is the apparent density of samples which is obtained by weighing the sample and dividing by its apparent volume. The results of particulate properties like X-ray density (D_X), measured apparent density (D) and porosity (P) of samples are given in Table II. It is noticed from this table that the X-ray densities, D_X (true densities) for all compositions of Cd-Ni ferrites decreases with nickel addition. The X-ray densities, D_X, are higher than the apparent density, D. This is attributed to the existence of the pores which depends on the sintering conditions. The nickel addition increases the porosity, thus reduces apparent density of the sample.

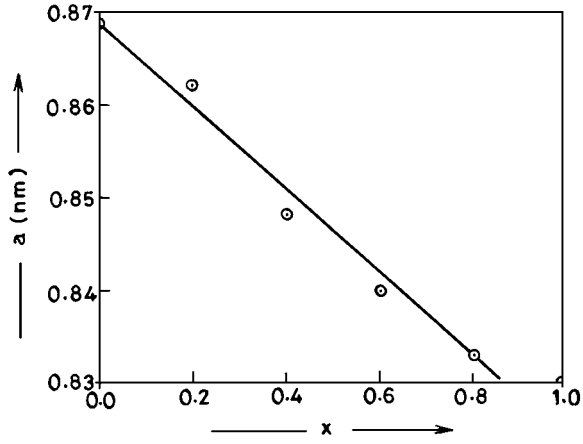

Figure 2 Variation of lattice parameter '*a*' as a function of composition *x*.

The crystallite sizes $\langle D\rangle_{\text{X-ray}}$ of these samples are also calculated from the full width at half-maximums of (220), (311) and (511) diffraction peaks using Debye–Scherrer formula [31]

$$\langle D\rangle_{\text{X-ray}} = \frac{0.94\lambda}{\beta \cdot \cos\theta}$$

where λ is the wavelength, β is the half-peak width and θ is the Bragg's angle. The observed mean values of the crystallite diameters $\langle D\rangle_{\text{X-ray}}$ are given in Table II. As can be seen from the Table II, the mean crystallite size for all compounds are in the range of 29.31 to 34.29 nm.

3.2.4. Infrared spectral studies

Infrared spectra of $Cd_{1-x}Ni_xFe_2O_4$ samples show two strong bands at ~580 and ~400 cm^{-1} and a poorly defined band at ~311 cm^{-1}. The band positions are listed in Table III. It can be easily noticed that no shift occurs in position of bands at frequency ν_2 and ν_3 by increasing the nickel content. Also, it can be seen that the frequency (ν_1) is shifted to higher frequencies with increasing nickel ion concentration and changes to $NiFe_2O_4$ (inverse spinel). In an inverse spinel, the octahedral site is occupied by Fe^{3+} and the divalent ion Ni^{2+}. Due to charge imbalance the oxygen ion is likely to shift towards the Fe^{3+} ion making the force constant between Fe^{3+} and O^{2-} more. Hence we expect an increase in band stretching mode as we go from normal spinel (i.e. $x = 0$) to inverse spinel (i.e. $x = 1$). The ν_3 band which appears in the samples containing

TABLE III Infrared spectroscopic bands for $Cd_{1-x}Ni_xFe_2O_4$ system ($0 \le x \le 1$)

Compounds	Absorption bands (cm^{-1})		
	ν_1	ν_2	ν_3
$CdFe_2O_4$	544	405	317
$Cd_{0.8}Ni_{0.2}Fe_2O_4$	556	402	315
$Cd_{0.6}Ni_{0.4}Fe_2O_4$	569	398	319
$Cd_{0.4}Ni_{0.6}Fe_2O_4$	580	399	321
$Cd_{0.2}Ni_{0.8}Fe_2O_4$	591	400	311
$NiFe_2O_4$	600	403	311

Cd^{2+} ions, could be assigned to Cd^{2+} tetrahedral vibration. Thus, it could be seen from Table III that the band ν_1 shifts to higher frequencies as the nickel content increases. This may be due to the change in the Fe^{3+}–O^{2-} stretching vibration.

The presence of Fe^{2+} ions in the ferrite can cause a shoulder or splitting of the absorption band [32]. Thus in the present studies on the infrared spectra of the $Cd_{1-x}Ni_xFe_2O_4$ samples reveal that the absorption band around ~580 cm^{-1} does not show any splitting or shoulders and the possibility of Fe^{2+} at the tetrahedral site is ruled out. There is evidence of weak splitting of the absorption band around 400 cm^{-1}, suggesting the possible presence of Fe^{2+} at the octahedral site, but this is not clearly established.

3.2.5. Electrical conductivity studies

3.2.5.1. Temperature dependence. The room temperature electrical conductivity values σ_{RT} for all the compounds of the system $Cd_{1-x}Ni_xFe_2O_4$ were found to vary between 10^{-8} and 10^{-9} Ω^{-1} cm^{-1}, for different values of x (Table IV). High conductivity values indicate that the elements with only one oxidation state are present at the B site. The $\log\sigma$ against T^{-1} plot (Fig. 3) of pure $CdFe_2O_4$, $NiFe_2O_4$ and mixed $Cd_{1-x}Ni_xFe_2O_4$ shows an initial decrease in electrical conductivity in the temperature range 333–416 K. The σ value then increases showing a definite kink (break) in the temperature range 645 to 806 K except for $CdFe_2O_4$ and $Cd_{0.8}Ni_{0.2}Fe_2O_4$, on further increase of temperature the σ value increases as temperature increases. The decrease in conductivity in the temperature range of 333 to 416 K (Table IV) corresponds to the desorption of adsorbed water molecules, usually adsorbed water molecule behaves as an electron donor. The kink

TABLE II Some physical parameters of $Cd_{1-x}Ni_xFe_2O_4$ system ($0 \le X \le 1$)

Compounds	Lattice parameter a (nm)	Mean crystallite size $\langle D\rangle_{\text{x-ray}}$ nm ±0.40	X-ray density D_x (g cm^{-3})	Apparent density D (g cm^{-3})	Porosity $P = 1 - D/D_x$
$CdFe_2O_4$	0.869	34.29	5.839	3.425	0.413
$Cd_{0.8}Ni_{0.2}Fe_2O_4$	0.862	32.12	5.751	3.341	0.419
$Cd_{0.6}Ni_{0.4}Fe_2O_4$	0.848	30.74	5.807	3.296	0.432
$Cd_{0.4}Ni_{0.6}Fe_2O_4$	0.840	31.61	5.734	3.171	0.446
$Cd_{0.2}Ni_{0.8}Fe_2O_4$	0.833	29.31	5.633	3.085	0.452
$NiFe_2O_4$	0.830	32.17	5.445	2.945	0.459

TABLE IV D. C. electrical conductivity data of $Cd_{1-x}Ni_xFe_2O_4$ system ($0 \leq x \leq 1$)

Compounds	Temperature, corresponding to desorption of adsorbed water (K)	σ at 500 K Ω^{-1} cm^{-1}	Activation energy E_a (eV)		Transition temperature (T_C) K
			Ferrimagnetic region	Paramagnetic region	
$CdFe_2O_4$	421	7.08×10^{-8}	–	0.700	–
$Cd_{0.8}Ni_{0.2}Fe_2O_4$	385	3.80×10^{-8}	–	0.710	–
$Cd_{0.6}Ni_{0.4}Fe_2O_4$	370	2.29×10^{-8}	0.496	0.760	645
$Cd_{0.4}Ni_{0.6}Fe_2O_4$	400	1.44×10^{-8}	0.571	0.799	667
$Cd_{0.2}Ni_{0.8}Fe_2O_4$	387	7.07×10^{-9}	0.628	0.862	714
$NiFe_2O_4$	416	3.80×10^{-9}	0.679	0.901	806

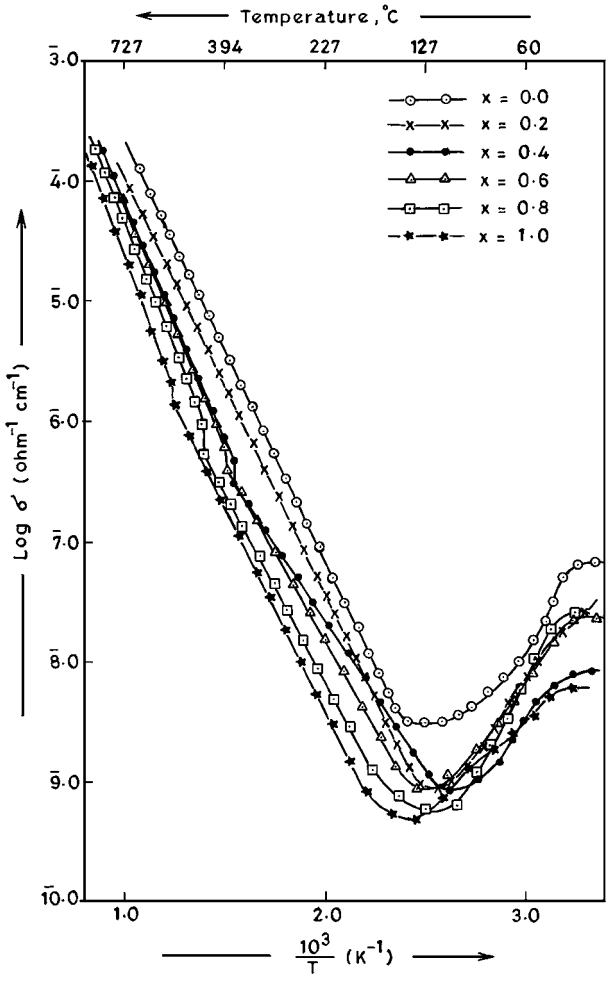

Figure 3 Plot of log σ against T^{-1} of $Cd_{1-x}Ni_xFe_2O_4$ system ($0 \leq x \leq 1$).

occurs in each curve ($x \geq 0.4$) at temperature which corresponds to ferrimagnetic (ordered state) to paramagnetic transition (disordered state). No such magnetic transformation was observed for the sample $CdFe_2O_4$ and $Cd_{0.8}Ni_{0.2}Fe_2O_4$, which suggest that these samples are paramagnetic at room temperature.

The two activation energies are calculated for the two regions around the kink points, firstly for ferrimagnetic and secondly for paramagnetic region. The observed values of the activation energies, E_a (eV) and T_C, for the series $Cd_{1-x}Ni_xFe_2O_4$ are listed in Table IV. It is interesting to observe here that the activation energy in the paramagnetic region is higher than that in the ferrimagnetic region. The behaviour of the activation energy on passing through T_C may be explained by the double exchange mechanism [33]. Hence the electrical conduction in the system under investigation is due to the electron hopping in the sublattices between $Fe^{2+} \rightleftharpoons Fe^{3+}$ ions and results increasing in activation energy in the paramagnetic region. This can also be attributed to disordered state of the paramagnetic region and ordered state of the ferrimagnetic region.

3.2.5.2. Composition dependence. The d.c. electrical conductivity i.e. σ measurement of $Cd_{1-x}Ni_xFe_2O_4$ ($0 \leq x \leq 1$) indicates that conductivity decreases as the nickel ion substitution increases (Table IV). This is due to fact that on increasing Ni^{2+} ion substitution (at B-site), the Cd^{2+} ion concentration (at A-site) will decrease. This leads to the migration of some Fe^{3+} ions from B-site to A-sites to substitute the increase of Ni^{2+} ion concentration at B-site. As a result, the number of ferrous and ferric ions at B-site decreases (which are responsible for electric conduction in ferrites). Consequently, conductivity decreases on increasing Ni^{2+} ion substitution. Another reason for the decrease in conductivity on increasing Ni^{2+} ion substitution is that nickel is more resistive ($\rho = 6.99\ \mu\ \Omega$ cm) than cadmium ($\rho = 6.83\ \mu\ \Omega$ cm) [34, 35].

The activation energies, Ea, of electronic conduction and transition temperature, T_C, were found to increase on increasing replacement of magnetic nickel ions to nonmagnetic cadmium ions. The increase of activation energy Ea and transition temperature T_C (Table IV) as Ni^{2+} ion substitution increases could be related to the same reasons for the decrease in the electrical conductivity. This result is in good accordance with the conclusion that the higher activation energy is associated with lower electrical conductivity [36]. The increase in Ea with increasing x (Table IV) can be interpreted in terms of their magnetic properties. The activation energy for $x = 0.0$ sample is much lower owing to very weak A-B interaction (Cd^{2+} ion non-magnetic). As nickel addition (x) increases in the $Cd_{1-x}Ni_xFe_2O_4$ mixed spinels, the antiferromagnetic order changes and enhances the activation energy for electrical conduction. Therefore, magnetic ordering changes might be responsible for the increase in activation energy.

3.2.5.3. Porosity dependence. The electrical conductivity (i.e. log σ at 500 K) was found to decrease as the porosity increases (see Tables II and IV). When the porosity increases the number of pores, vacancies and scattering centers for the electric charge carriers

increases, as a result a marked decrease in the electrical conductivity will be produced. It has been reported [37] that the pores may or may not be filled by air; but these pores invariably introduce the insulating or the impeding paths to the electrons. In other words, these pores offer extrinsic contribution to the activation energy. The increase in activation energy (E_a) may be attributed to the increase in number of grains. Due to the increased number of pores, the individual grain to grain contact decreases. The resistivity is inversely proportional to the cross sectional area of the conductor and total conduction of the matrix may decrease. Reduction in conductivity is just the consequence of increase in activation energy. Therefore, the conductivity of a polycrystalline material in general decreases with decreasing grain size [37].

3.2.6. Thermoelectric power measurements

The thermoelectric power (TEP) measurements for $Cd_{1-x}Ni_xFe_2O_4$ system are illustrated in Fig. 4. It shows as initial fall in number of charge carriers (negative charge carriers) in the temperature range upto 450 K and then the number (negative thermoelectric power) increases continuously with increase of temperature. It has been well established [38] that in case spinel type compounds, the distance between the tetrahedral (A) -tetrahedral (A) site ion is too large and no overlap of wavefunction of the A-site ion takes place. The probability of electrons jumping in the A-site sublattice is therefore negligible and it can be assumed that no conduction take place by the jumping of the charge carriers at these sites. All conduction is therefore attributed to the hopping of the charge carriers from one octahedral (B) ion to another octahedral (B) ion.

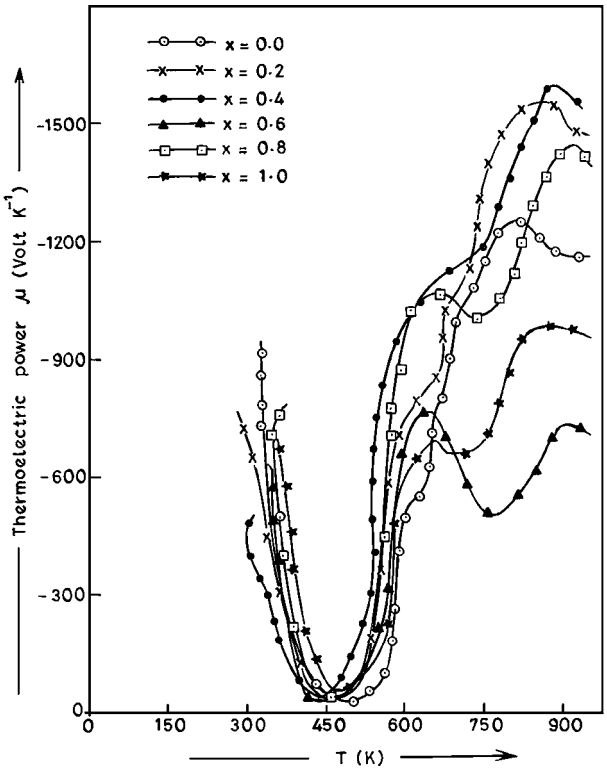

Figure 4 Plot of Thermoelectric power, μ (volt K^{-1}) against T (K) of $Cd_{1-x}Ni_xFe_2O_4$ system ($0 \leq x \leq 1$).

The common feature for all compositions is that, thermoelectric power is negative over the whole range of temperature, indicating that the charge carriers are electrons. Increase in magnitude of TEP with temperature might be due to activated electron hopping between Fe^{2+} and Fe^{3+}. Verwey and deBoer [39] have established that in oxides, containing one ion of variable valence, the conduction takes place by hopping via activation of states involving cations changing valence as $Fe^{2+} \rightleftharpoons Fe^{3+}$ and vice versa. The presence of nickel ion at the octahedral sites favours the conduction mechanism as proposed by Van Uitert [40], viz.

$$Ni^{2+} + Fe^{3+} \rightleftharpoons Ni^{3+} + Fe^{2+}$$

which explains the predominant conduction mechanism of nickel–cadmium system under investigation. Thus the conduction mechanism is of n-type for all samples which is due to the hopping of electrons from Fe^{2+} to Fe^{3+} ions.

3.2.7. Magnetic studies

The compounds of the system $Cd_{1-x}Ni_xFe_2O_4$ with $x \geq 0.4$ studied in the present work showed a definite hysteresis loop at room temperature, which indicates the ferrimagnetic behaviour. From the hyteresis loops, the coercive force (H_C), saturation magnetization (M_S) and ratio of remanance to saturation magnetization (M_R/M_S), magnetic moment (n_B) and YK angles (θ_{YK}) values have been calculated and are listed in Table V. The compounds with $x = 0.0$ and 0.2 do not show hysteresis loops, indicating that these ferrites are of antiferromagnetic in nature. Therefore we did not observe any magnetization for a composition $x = 0.2$ at room temperature; it may be consisted of a mixture of paramagnetic phase (as the major phase) and a small amount of a ferrimagnetic phase. However, it was verified by an alternate check by experimantally determining magnetization at liquid nitrogen temperature. At this low temperature the saturation magnetization (M_S) was observed for this sample (12.5 emu g^{-1}).

From Table V it is seen that as the content of nickel is increased, the value of saturation magnetization also shows increasing trend upto $x = 0.6$, beyond which a decreasing trend is exhibited. The variation of magnetization of such samples ($x \geq 0.4$) can be explained on Néel's two sublattice models of ferrimagnetism [41]. The introduction of nickel ions which have a strong preference for the spinel at B-site and the cation distribution is given by

$$\left(Cd^{2+}_{1-x}Fe^{3+}_{x}\right)_A\left[Fe^{3+}_{2-x}Ni^{2+}_{x}\right]_B O^{2-}_4$$

where the ions enclosed by round brackets correspond to tetrahedral or A-site and the ions enclosed by square brackets corresponds to octahedral or B-site. This cation distribution is presented from the fact that Cd^{2+} is a non-magnetic ion and has strong preference for A-site [42]. On the other hand Ni^{2+} has strong preference for B-site [43]. On going to B-site it forces equal number of Fe^{3+} ions to A-site. The calculated

TABLE V Magnetic properties and curie temperature (T_C) for $Cd_{1-x}Ni_xFe_2O_4$ system ($0 \leq X \leq 1$)

Compounds	Coercive force (H_C) ± 0.5 Oe	Saturation magnetisation (M_s) ± 2 emu g^{-1}	Ratio of M_R/M_S	Magnetic moment $n_B \pm 0.1$ BM		Curie temperature (T_C) ± 5 K	⟨θ° YK⟩ angles observed
				Observed	Calculated		
$Cd_{0.6}Ni_{0.4}Fe_2O_4$	57.60	45.72	0.53	2.18	8.236	639	56°.63′
$Cd_{0.4}Ni_{0.6}Fe_2O_4$	102.00	68.64	0.50	3.14	6.434	658	33°.92′
$Cd_{0.2}Ni_{0.8}Fe_2O_4$	96.00	58.64	0.55	2.57	4.632	705	24°.14′
$NiFe_2O_4$	72.00	52.39	0.57	2.19	2.830	798	0.0°

and observed magnetic moment are evaluated [19] and are given in Table V. The observed net magnetic moment n_B values are compaired with the calculated n_B values on the basis of spin-only moments of Néel's [41] two sub-lattice model (Table V). It has been observed as in case of $x = 1$, the observed magnetic moments (n_B) is slightly less then the calculated one. This small variation may be due to the preparation technique.

The Neel's two sublattice model can be applied for this sample. The observer n_B value for $x \leq 0.8$ are lower than the calculated n_B values (Table V). This low magnetic moments can be explained in terms of the non-collinear spin arrangement i.e. the presence of a small canting of the B-site moment with respect to the direction of the A-site moment [44, 45]. The Yafet–Kittel angles $\langle\theta^\circ_{YK}\rangle$ were calculated using the formula [18, 45]

$$\mathrm{Cos}\,\theta_{YK} = \frac{n_B + 5(1-x)}{7+x}$$

where n_B is expressed in the units of Bohr-magneton and x represents the contents of cadmium. The observed Y-K angle are listed in Table V. It is seen that the Y-K angle goes on decreasing upto the samples $x = 0.8$. The decrease in Y-K angles indicate the decreasing favouring of triangular spin arrangement on B-sites leading to an increase in A-B interaction. Thus the observed variation of the magnetization upto $x = 0.8$, which has been explained on the bases of the existence of Yafet–Kittel angles on the B-site spins. Furthermore, it is also possible to correlate the observed magnetization (n_B) to porosity (P) of these samples (see Table II). A pore is sort of void or a gap and this will break up the magnetic circuit between grain to grain. If the number of pores is large this may lead to the net reduction of magnetization in the bulk. The grain boundary acts as an obstacle for the domain wall motion or rotation due to large number of grains per c.c, the net area of the grain boundary increases and thus greater resistance for the process of magnetization is observed. Besides, when there are more pores the probability of occurrence of closed pore chains increases leading to reduction of magnetization This view is supported by the work of Rikukawa [46].

The coercive force (H_C) and the remanence ratio (M_R/M_S) for all compounds ($x \geq 0.4$) are comparable (Table V), which indicate that the anisotropy character for all samples are similar in nature. It is interesting to observe that, for all samples the M_R/M_S ratio are also comparable with the mean crystallite size (see Table II).

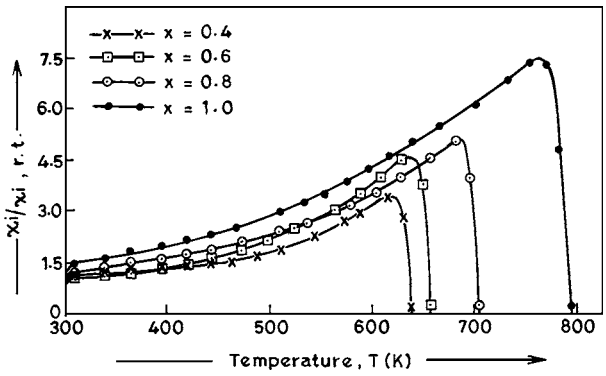

Figure 5 Plot of χ_i/χ_i, *r.t* against temperature (T) for the system $Cd_{1-x}Ni_xFe_2O_4$ ($0 \leq x \leq 1$).

The M_R/M_S the ratio of all compounds are greater than 0.5, which indicate the magnetic behaviour of system approaches that of a random system of non-interacting single-domain particles with cubic anisotropy.

3.2.8. Initial magnetic susceptibility measurements

The study of the temperature variation of initial magnetic susceptibility (χ_i) curves of $Cd_{1-x}Ni_xFe_2O_4$, with $x \geq 0.4$, compounds show a typical Hopkinson effect [47]. For these samples χ_i increases with increasing temperature giving a peak value and then suddenly becomes zero just before the Curie temperature (Fig. 5). This is a characteristic behaviour of sample having a single domain grains. The Curie temperature T_C for $x \geq 0.4$ compounds are determined from these curve and are listed in Table V. T_C values are found to increase with increasing Ni^{2+} concentration at B-site, probably due to the strengthening of A-B interactions. The increase of T_C can be well correlated with the observed values of Y-K angle in the ferrites (Table V). Y-K angles decreases on increasing Ni^{2+} concentration, and it is characterised by a increase in A-B interaction leading to increase of T_C in the ferrites.

The absence of multi-domain grains is supported by the fact that Hopkinson's effect was not observed. The χ_i verses t curve of superparamagnetic samples show χ_i decrease as T increases [48].

3.2.9. Mössbauer studies

The room temperature Mössbauer spectra of $Cd_{1-x}Ni_xFe_2O_4$ system with $x = 0.0$ to 1.0 are shown in Fig. 6 and spectral parameters such as isomer

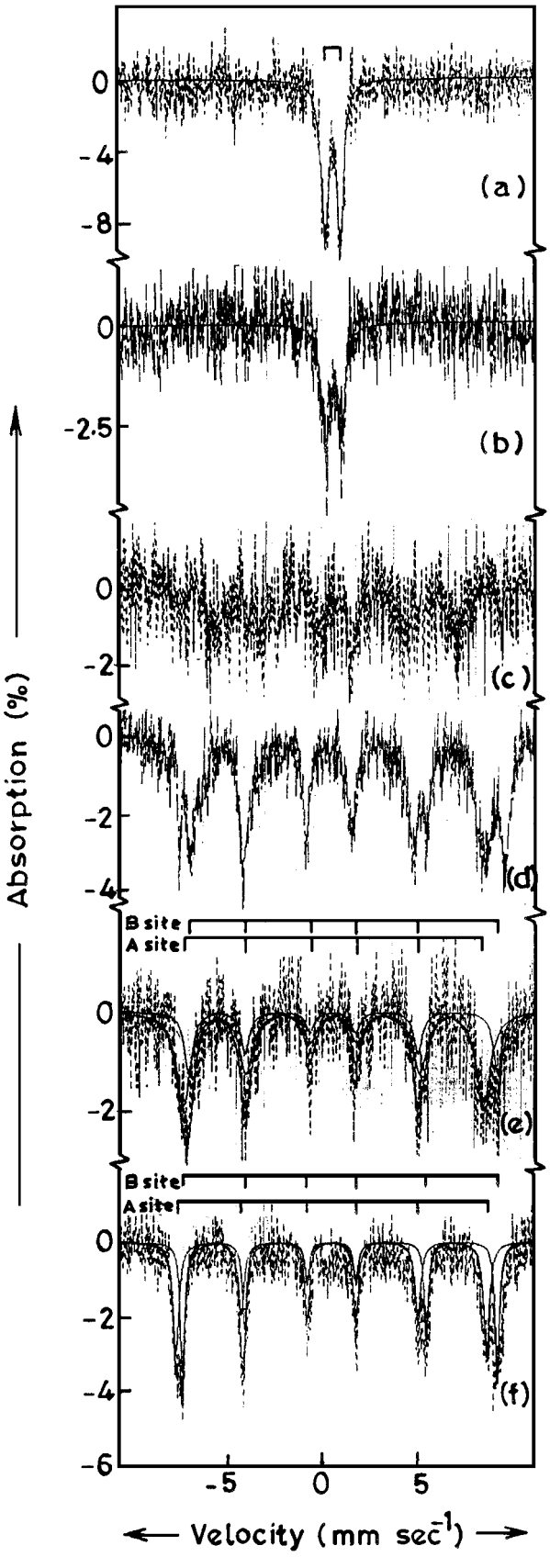

Figure 6 Mössbauer spectra at room temperature of the $Cd_{1-x}Ni_x Fe_2O_4$ system ($0 \leq x \leq 1$).

shift (δ), quadrupole splitting (Δ EQ) and hyperfine fields (Hn) at A and B sites are computed and are summarized in Table VI. In the Fig. 6, the mark points represent the experimental points and two continuous lines through the data point are results of the least square fit to the data of the two mixed magnetic dipole and electric quadrupole ^{57}Fe hyperfine patterns of each other.

The Mössbauer spectra of $Cd_{1-x}Ni_xFe_2O_4$ with $x = 0$ to 0.2 (Fig. 6) are paramagnetic at room Temperature. In case of the sample $x = 0$ (i.e. $CdFe_2O_4$) it is a perfect normal spinel, all Fe^{3+} ions occupy B-sites where trigonal field is present [48]. The trigonal field distorts the octahedron formed by six O^{2-} ions around the B-sites, changing the symmetry locally from perfect cubic. This would then cause an electric field gradient at the Fe^{3+} nucleus, leading to quadrupole doublet. For the compositions, $Cd_{0.8}Ni_{0.2}Fe_2O_4$ (i.e. $x = 0.2$) there is small percentage of Fe^{3+} ions at A sites, which do not experience any electric field gradient due to cubic symmetry of this site. Hence spectrum has been split into a singlet arising from A-site, and a doublet corresponding to B-site iron. However, for $x = 0.2$ showed no saturation magnetization, this is due to the sample consisted of a paramagnetic as the major phase or more probably, that instead of ferrimagnetic particles in this case ferromagnetic region exist which are separated magnetically from the matrix, since the region is surrounded by diamagnetic Cd^{2+} ions. Therefore, this sample ($x = 0.2$) shows paramagnetic doublets i.e. no distinct evaluation of the hyperfine field observed.

In case of samples with ($x = 0.4$ and 0.6) at room temperature show a relaxation behaviour. The primary features of a relaxation spectrum for a magnetically ordered system are significant broadening of Zeeman lines and a growth of the inner lines of the Zeeman patterns at the expense of the outer lines. Both these effects are evident in the Mössbauer spectrums obtained with $x = 0.4$ and 0.6. The observed Mössbauer spectrum is a super position of the two magnetically split sextets and a relaxed quadrupole doublet arising due to the domain wall oscillation effects. Panicker *et al.* [49] found that the relaxation effect in Mössbauer line shapes are due to domain wall oscillation. Therefore it is not possible to draw any quantitative conclusion about the Mössbauer parameters.

The Mössbauer spectra of $Cd_{1-x}Ni_xFe_2O_4$ samples with $x \geq 0.8$ (Fig. 6) exhibit normal Zeeman split sextets, one due to Fe^{3+} ions at the tetrahedral (A) sites and the other due to Fe^{3+} ions at the octahedral (B) sites. The isomer shift show very little change (Table VI) with Ni^{2+} content up to $0.0 \leq x \leq 0.2$, indicating that the s-electron distribution of Fe^{3+} ions is practically not influence by Ni^{2+} substitution. It is also apparent from Table VI that $x = 0.8$ to 1.0 have significant variation of isomer shifts for Fe^{3+} ions at A and B site. This indicates that the s-electron distribution of the Fe^{3+} ions is very much influenced by Ni^{2+} substitution at B-site.

The quadrupole splitting decreases when nickel is progressively added into $CdFe_2O_4$ (Table VI). We explain our observed reduction in quadrupole splitting in the following way. As mentioned earlier the quadrupole splitting at the B-site is due to presence of the trigonal field. It is well known that $NiFe_2O_4$ is a completely inverse spinel. The Ni^{2+} ions occupy the B-sites and Fe^{3+} ions are distributed equally over A and B-sites. $CdFe_2O_4$ on the other hand is a normal spinel with Cd^{2+} at tetrahedral site and Fe^{3+} at octahedral sites.

TABLE VI Mössbauer parameter for $Cd_{1-x}Ni_xFe_2O_4$ system ($0 \leq x \leq 1$)

Compounds	Site	Isomer shift[a], (δ) ($\pm$ 0.02 mm sec^{-1})	Quadrupole splitting, ($\triangle$ EQ) ($\pm$ 0.02 mm sec^{-1})	Hyperfine field, (Hn) ($\pm$ 5.0 KOe)
$CdFe_2O_4$	–	0.401	0.800	–
$Ni_{0.2}Cd_{0.8}Fe_2O_4$	–	0.379	0.807	–
$Ni_{0.4}Cd_{0.6}Fe_2O_4$	}	Relaxation spectra		
$Ni_{0.6}Cd_{0.4}Fe_2O_4$	}			
$Ni_{0.8}Cd_{0.2}Fe_2O_4$	A	0.337	0.017	492
	B	0.547	0.292	505
$NiFe_2O_4$	A	0.280	0.049	508
	B	0.652	0.127	516

[a]With respect to natural iron metal.

Therefore in mixed $Cd_{1-x}Ni_xFe_2O_4$ system, the A-sites are occupied by Cd^{2+} and Fe^{3+} ions and the B-sites by Ni^{2+} and Fe^{3+} ions. As we go from $CdFe_2O_4$ ($x = 0.0$) to $NiFe_2O_4$ ($x = 1.0$), A-site Cd^{2+} ions are gradually replaced by Fe^{3+} ions. The replacement of the large Cd^{2+} ions (0.097 nm) by the small Fe^{3+} ions (0.065 nm) at the tetrahedral sites distorts the oxygen octahedron around the B-site largely, thereby increasing the field gradient at the B-site considerably. The displacement of oxygen ions around the A-site caused by the replacement of Cd^{2+} by Fe^{3+} ions is such that the cubic symmetry of this site is retained. The distortion in the B-site octahedron is evidenced by the change in the oxygen parameter, u, from $CdFe_2O_4$ to $NiFe_2O_4$. The recently reported values of u are 0.389 ± 0.005 [50] and 0.382 ± 0.003 [51] for $CdFe_2O_4$ to $NiFe_2O_4$ respectively. Therefore it is proposed that the decrease in quadrupole splitting from $CdFe_2O_4$ to $NiFe_2O_4$ is ascribed to the decrease in the u value (the distortion parameter of the anion sublattice).

The observed variation of A and B site hyperfine fields (Hn) with the nickel concentration ($x \geq 0.8$) is given in Table VI. It is seen that hyperfine field increases with increasing nickel content. This is attributed to exclusive octahedral site occupation of Ni^{2+} ions. The B-site hyperfine fields are higher than A-site because of increasing magnetization of the B sublattice. The magnetic measurements also confirm these results. It is also apparent that A-site hyperfine field (H_A) increases faster than B-site hyperfine field (H_B) (Table VI). This may be possible due to a change in spin space orientations in nickel substituted ferrites. It is interesting to observe that with increasing x (i.e. Ni^{2+} ion concentration), the lattice parameter decreases and the overlap of electron wave function of Fe^{3+} ions and O^{2-} ions increases and the hyperfine field increases. Since with increase in Ni^{2+} content the mean splitting increases (as the Curie temperature does, the magnetic coupling strengthens the A-B interaction). Thus the sextets with a higher magnetic splitting (H_B) belong to Fe^{3+} environments in which the number of neighbouring Ni^{2+} is larger (i.e. superexchange interactions Fe^{3+}—O—Ni^{2+} increases). This supports that the triangular (canted) spin arrangement (i.e. Yafet–Kittel angles) are present in $Cd_{1-x}Ni_xFe_2O_4$ system upto, $x = 0.8$ which suggests that B-B and A-B superexchange interactions are comparable in strength. The Néel's two sublattice model may be applicable upto $x > 0.8$ nickel content.

Thus, from all the above measurements, we prefer the following configuration for $Cd_{1-x}Ni_xFe_2O_4$ system ($0 \leq x \leq 1$):

$$\left(Cd^{2+}_{1-x}Fe^{3+}_{x}\right)_A\left[Fe^{3+}_{2-x}Ni^{2+}_{x}\right]_B O^{2-}_4$$

4. Conclusions

(a) X-ray powder diffraction pattern of ferrispinels such as $Cd_{1-x}Ni_xFe_2O_4$ compounds possesses a spinel structure. The lattice parameter decreases linearly with the increase of nickel concentration in these samples. The particulate properties like X-ray density and apparent density decreases while porosity increases as a function of composition for $Cd_{1-x}Ni_xFe_2O_4$ samples. The mean crystallite size for all samples did not show any trend as x increases.

(b) Temperature variation of d. c. electrical conductivity for all samples show a definite kink in the range 645 to 806 K except for pure $CdFe_2O_4$ and $Cd_{0.8}Ni_{0.2}Fe_2O_4$ samples, which corresponds to ferrimagnetic to paramagnetic transition. The conductivity decreases as the nickel ion substitution increases. The activation energies (E_a) for electrical conduction and the transition temperature (T_C) were found to increase as nickel ion substitution increases. Similarly, the electrical conductivity decreases as the porosity increases.

(c) The compounds of the system $Cd_{1-x}Ni_xFe_2O_4$ with $x \geq 0.4$ showed a definite hysteresis loop. The composition dependence of magnetization (i.e., M_S and n_B) upto $x = 0.8$, which has been explained on the basis of the existence of Yafet–Kittel angles on the B-site spins. The Néels two sublattice model can applied for the sample $x = 1$. The coercive force (H_C) and (M_R/M_S) ratio for all compounds ($x = 0.4$) are comparable, which indicate that the anisotropy character for all samples are similar in nature.

(d) The data on the temperature variation of the initial magnetic susceptibility suggest that these samples have single domain grains. The Curie temperature are found to increase with increasing Ni^{2+} content.

(e) The Mössbauer spectra of $Cd_{1-x}Ni_xFe_2O_4$ with $x = 0.0$ to 0.2 shows a paramagnetic doublet while $x = 0.4$ and 0.6 exhibits a relaxation spectrum. The samples with $x \geq 0.8$ exhibit normal Zeeman split sextets at room temperature. The systematic increase in hyperfine field at both sites and the rapid increase at tetrahedral (A) site as compared to that at octahedral (B) site in $x \geq 0.8$ sample has been suggested that

the magnetic coupling strengthens A-B interactions. The canted spin arrangement may be present in these compounds.

(f) By means of the structural, electrical, magnetic and Mössbauer results, the cation distribution has been found to be

$$\left(Cd^{2+}_{1-x}Fe^{3+}_{x}\right)_{A}\left[Fe^{3+}_{2-x}Ni^{2+}_{x}\right]_{B}O^{2-}_{4}$$

Acknowledgements

This work was supported by U.G.C., New Delhi. The teacher fellowship scheme (AVN) was awarded.

References

1. N. BURRIESCI, F. GARBASSI and S. PIZZINI, *J. Magn. Magn. Mater.* **7** (1978) 52.
2. A. GLOBUS, H. PASCARD and V. CAGAN, *J. Physique Colloq.* **38** (1977) C1.
3. N. A. EISSA, A. A. BAHGAT and M. K. FAYEK, *J. Phys. F : Metal Phys.* **7** (1977) 2209.
4. J. FONTCUBERTA, J. RODRIGUEZ, M. P. I. R. RODRIGUES and J. TEJADA, *Mater. Res. Bull.* **15** (1980) 969.
5. E. WOLSKA, W. WOLSKI, J. KACZMAREK, E. RIEDEL and D. PRICK, *Solid State Ionics* **51** (1992) 231.
6. *Idem., ibid.* **101** (1997) 1069.
7. M. A. AMER and O. M. HAMADA, *Hyperfine Interact.* **96** (1995) 99.
8. D. RAVINDER and T. ALIVELU MANGA, *Mater. Lett.* **41** (1999) 254.
9. A. WOLD, *J. Chem. Educ.* **57** (1980) 531.
10. J. TIRADO, J. M. THOMAS, D. A. JEFFERSON, G. R. MILLWARD and S. W. CHARLES, *J. Chem. Soc. Chem. Commun.* (1987) 365.
11. S. KARMARNENI, E. FREGEAU, E. BREVAL and R. ROY, *J. Amer. Ceram. Soc.* **71**(1) (1988) C26.
12. B. GILLOT, M. EL. GUENDOUZI, A. ROUSSET and P. TAILHADES, *J. Mater. Sci.* **21** (1986) 2926.
13. P. PESHEV, A. TOSHEV and G. GYUROV, *Mat. Res. Bull.* **24** (1989) 33.
14. K. VIDYASAGAR, J. GOPALKRISHNAN and C. N. R. RAO, *Inorg. Chem.* **23** (1984) 1206.
15. L. MARKOV and L. PETROV, *Reactive Solids* **1** (1986) 319.
16. P. RAVINDRANATHAN, G. V. MAHESH and K. C. PATIL, *J. Solid State Chem.* **66** (1987) 20.
17. B. A. BENDER, R. W. RICE and J. R. SPANN, *J. Amer. Ceram Soc.* **70**(3) (1987) C58.
18. V. G. PANICKER, R. V. UPADHYAY, S. N. RAO and R. G. KULKARNI, *J. Mater. Sci. Lett.* **3** (1984) 385.
19. A. K. NIKUMBH, A. V. NAGAWADE, V. B. TADKE and P. P. BAKARE, *J. Mater. Sci.* **36** (2001) 653.
20. M. J. BUERGER, "Crystal Structure Analysis" (New York, Wiley, 1960) p. 46.
21. S. D. LITHITE, C. RADHAKRISHNAMURTHY and P. W. SAHASRABUDHE, *Rev. Sci. Instrum.* **36** (1965) 1558.
22. S. D. LITHITE and C. RADHAKRISHNAMURTHY, *Bulletin National Geophysical Research Institute* **3** (1965) 1.
23. C. RADHAKRISHNAMURTHY, S. D. LITHITE, B. S. AMIN and B. L. K. SOMAYAJULU, *Earth Palnet Sci. Lett.* **4** (1968) 464.
24. S. KRISHNER and R. KIASLING, *J. Am. Chem. Soc.* **82** (1960) 4174.
25. J. R. ALLAN, H. J. BOWLEY, D. L. GERRAD, A. D. PASTON and K. TURVEY, *Thermochimica Acta* **124** (1988) 345.
26. ASTM File number, **22**-1063.
27. ASTM File number, **10**-325.
28. A. A. GHANI and A. A. SATTAR, *J. Magn. and Magn. Mat.* **97** (1991) 141.
29. C. G. WHINFREG, D. W. ECKART and A. TAUDER, *J. Am. Chem. Soc.* **82** (1960) 2695.
30. D. C. KHAN, M. MISHRA and A. R. DAS, *J. Appl. Phys.* **53** (1982) 2772.
31. H. P. KLUG and L. E. ALEXANDER, "X-ray Diffraction Procedure" (Wiley Interscience, New York, 1954) Ch. 9.
32. O. S. JOSYULU and J. SOBHANDRI, *Phys. Stat. Solidi* (a) **65** (1981) 479.
33. YU. P. IRKHIN and E. A. TUROV, *Sov. Phys - JETP* **33** (1957) 673.
34. C. KITTEL, "An Introduction to Solid State Physics" 5th edn. (Wliey, London/New York, 1976) p. 170.
35. CRC Handbook of Chemistry and Physics, 61st edn.
36. J. SMIT and H. P. J. WIJN, "Ferrites" (Philips Tehnical Library, Eindhoven, the Netherlands, 1959).
37. W. D. KINGERY, H. K. BOWEN and D. R. UHLMANN, "Introduction to Ceramics" (Wiley, New York, 1975) p. 904.
38. E. J. W. VERWEY, "Semiconducting Materials" edited by H. K. Henigh (1951).
39. E. J. W. VERWEY and J. H. DE BOER, *Recl. Trav. Chim. Pays-Bas (Netherlands)* **55** (1936) 531.
40. L. G. VAN UITERT, *J. Chem. Phys. (USA)* **24** (1956) 306.
41. L. NÉEL, *Ann. Phys.* **3** (1948) 137.
42. G. BLASSE, *Philips Res. Rept.* **3** (1964) 1.
43. G. JOSHI, A. KHOT and S. SAWANT, *Solid State Commun.* **65** (1988) 1593.
44. J. B. GOODENOUGH, *Prog. Solid State Chem.* **5** (1971) 146.
45. Y. YAFET and C. KITTEL, *Phys. Rev.* **87** (1952) 290.
46. H. RIKUKAWA, *IEEE Trans. Magn. (USA)* **18** (1982) 1535.
47. J. HOPKINSON, *Phil. Trans. R. S. (London)* **A180** (1889) 443.
48. J. SMIT, F. K. LOTGERING and R. P. VANSTAPELE, *J. Phys. Soc., Japan* **17** (1962) 268.
49. V. G. PANICKER, S. N. RAO and R. G. KULKARNI, *Solid State Commun.* **43** (1982) 647.
50. B. J. EVANS, S. S. HAFNER and H. P. WEBER, *J. Chem. Phys.* **55** (1971) 5282.
51. S. I. YOUSSEF, M. G. NATERA, R. J. BEGUM, B. S. SHRINIVASAN and N. S. SATYAMURTHY, *J. Phys. Chem. Solids* **30** (1969) 1941.

Received 29 June 2000
and accepted 1 October 2001